Lab on a Chip

PAPER

View Article Online
View Journal | View Issue

Cite this: *Lab Chip*, 2015, **15**, 2460

Frequency modulated microrheology†

Matthew M. Shindel and Eric M. Furst*

Received 24th March 2015,
Accepted 17th April 2015

DOI: 10.1039/c5lc00351b

www.rsc.org/loc

Coupling analog frequency modulation (FM) to the driving stimulus in active microrheology measurements conducted with optical tweezers effectively parallelizes numerous single-frequency experiments. Consequently, frequency modulated microrheology (FMMR) can efficiently characterize the dynamic stress response of complex fluids over several frequency decades in a single experiment. The time required to complete an FMMR measurement scales with the lowest frequency probed, improving throughput over the serial frequency sweep approach. The ease of implementation, straight-forward data analysis and rapidity of FMMR offer particular utility toward applications such as characterization of non-equilibrium materials, automated microrheology instrumentation, high-throughput screening of biomaterials and (bio) pharmaceutical formulations, and *in situ* monitoring of chemical and biochemical reaction processes.

Introduction

Microrheology encompasses a suite of characterization tools that evaluate the stress response of complex fluids through analysis of the motion of embedded microscopic particles.[1] Compared with traditional bulk techniques, the functional and practical advantages offered by microscopic forms of rheometry include small sample volumes (~1–50 μl), wide dynamic response (10^0–10^6 Hz), the capacity for local, global, and interfacial measurements, and the ability to incorporate the measurement into microfluidic devices.[2] Microrheology is highly amenable to numerous applications in emerging areas of bio- and nanotechnology, particularly in instances where the materials of interest are scarce or difficult to obtain.[3–7] Consequently, the development of microrheology methods that are increasingly easy to perform or serve as the operational kernel for automated instrumentation, will significantly benefit a variety of industries, as well as areas of active research and development, such as pharmaceuticals, polymer materials, and consumer care products.

Microrheology measurements can be either passive or active. Passive microrheology relies on the diffusive motion of Brownian probes. Linear viscoelastic properties are extracted from the ensemble-averaged mean-square-displacement (MSD) of a probe population or from the MSD of a single probe confined by a localized potential field.[8,9] The frequency range evaluated in a single measurement is bounded above by the bandwidth of the particle tracking method, and below by and total observation time. A material's constitutive stress response can also be determined by actively driving a colloidal probe within the host material *via* an external stimulus (active microrheology), commonly comprised by an optical or magnetic force.[10–16] Similar to bulk rheometry, frequency sweeps (FS) are commonly used in active microrheology to discern storage and loss moduli piecewise, through consecutive application of an oscillatory driving force (mechanical, optical, electrokinetic, magnetic or otherwise). The oscillation frequency is sequentially stepped between discrete values in order to probe viscoelasticity over the desired spectral range.[17–19] Although effective, sweeps are relatively laborious and become more time-consuming with increasing frequency resolution.

Alternatively, non-oscillatory approaches to microrheology have been devised with optical tweezers to provide broadband rheological characterization. Stochastic optical active rheology (SOAR) uses Gaussian noise to randomly displace an optical trap, extracting local viscoelastic properties from the psuedo-thermal motion of the probe.[20] Wideband microrheology, formulated by Preece *et al.*, examines the probe's

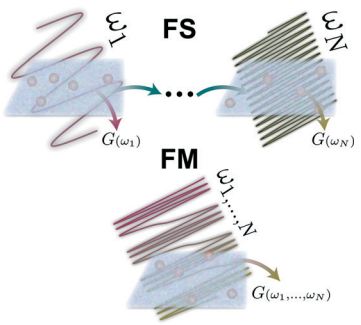

Fig. 1 Illustration of the frequency sweep (FS) and frequency modulation (FM) methods of active microrheology.

University of Delaware, Chemical and Biomolecular Engineering, Center for Molecular and Engineering Thermodynamics, 150 Academy St., Newark, Delaware, USA. E-mail: furst@udel.edu; Tel: +1 302 831 0102

† Electronic supplementary information (ESI) available: See DOI: 10.1039/c5lc00351b

step-response to discern the complex modulus of the surrounding environment.[21]

Frequency modulation (FM), the processes of encoding a signal *via* instantaneous frequency variations of a carrier wave, provides an additional route toward high-throughput active microrheology. Frequency modulated microrheology (FMMR) uses FM signal processing to construct a multimodal, oscillatory driving force, with constant amplitude and frequency components that span the spectral range of interest. The majority of the input signal's energy is discretely accumulated in select harmonics, enabling parallelized evaluation of the host material's rheology (Fig. 1). The equivalent FM bulk rheology method, termed "multiwave rheology" or Fourier-transform mechanical spectroscopy has been particularly useful for capturing the evolution of gelators and other materials with time-dependent rheology.[22,23]

Frequency modulation has a well-developed analytical framework due to its prominence in fields such as telecommunications, radar and telemetry, enabling straight-forward analysis of measurement data. This breadth in usage has also spawned an abundance of hardware and software utilities for synthesizing FM signals. Consequently, the resources required to implement FMMR are easily integrated with active microrheology instrumentation, including optical and magnetic tweezers.

This work provides an overview of the theory, experimental implementation and Fourier-based data analysis for FMMR. The technique is empirically validated in model Newtonian and viscoelastic fluids using optical tweezers. Measurement results from a recombinant human collagen solution are also presented. Finally, simulations in a generalized Maxwell fluid are used to compare settling times for FM and FS measurements.

Methods

Sample preparation

FMMR measurements were performed in Milli-Q filtered water and a 5% w/w aqueous solution of 200 kDa poly(ethylene oxide) (PEO; Sigma) containing 1.6 μm diameter polystyrene microparticles ($\phi < 10^{-4}$; Invitrogen). Samples were prepared in cells consisting of a glass coverslip (no. 1.5) and microscope slide joined with double-sided tape, and sealed with UV curable glue after loading, as described previously.[24]

Optical tweezer microrheology

Microrheological measurements were performed using a laser tweezer system (Fig. 2) described previously.[24] Briefly, an optical trap is generated by focusing a Nd–YAG laser (λ = 1064 nm; Coherent) to a diffraction limited spot with a 63× water-immersion objective (N.A 1.2). The trap is steered with an orthogonal pair of acousto-optic deflectors (AOD; A&A Optoelectronic). The particle's displacement from the optical trap is tracked interferometrically by imaging the condenser's back-focal-plane onto a quadrant photodiode (QPD; First Sensor).[25] Sequential Impulse Response (SIR) is

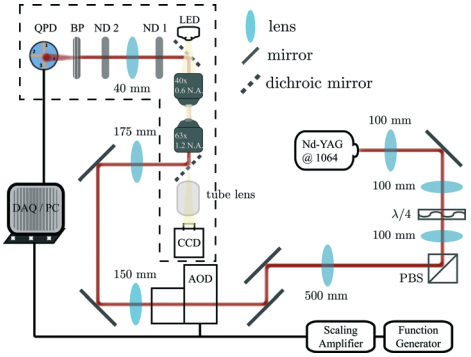

Fig. 2 Optical tweezer schematic. Dashed outline represents the microscope.

used to calibrate trap stiffness and detector sensitivity for each measurement.[24]

The FM drive signal is synthesized by a function generator (Agilent 33220A), and offset with a DC voltage added by a scaling amplifier (SRS). The relative position of the optical trap, $X(t)$, is given by a frequency modulated sinusoid with amplitude A.

$$X(t) = A\sin\left(2\pi\omega_c t + \int_0^t 2\pi\omega_\Delta \cos\left(2\pi\omega_m \tau\right)\mathrm{d}\tau\right)$$
$$X(t) = A\sin\left(2\pi\mathcal{C}\omega_m t + \mathcal{M}\sin\left(2\pi\omega_m t\right)\right) \quad (1)$$

ω_c and ω_m denote the carrier and modulation frequencies, respectively. The maximum instantaneous frequency deviation is given by ω_Δ, while the ratio ω_Δ/ω_m defines the modulation index $\mathcal{M}$. Similarly, the carrier index is given by $\mathcal{C} = \omega_c/\omega_m$. Trap position and probe displacement were recorded with a data-acquisition card (National Instruments PCI-6221), at a rate of 40 kHz. All measurements were performed at T = 22 °C.

Data analysis

Neglecting inertial effects, the probe's dynamic behavior is modeled by a modified Langevin equation.

$$0 = -\int_{-\infty}^{t} R(t-\tau)(\dot{w}(t) + \dot{X}(t))\mathrm{d}\tau - \kappa w(t) + F_B(t) \quad (2)$$

The probe's displacement from the trap is represented by $w(t)$, while κ $R(t)$ and $F_B(t)$ denote trap stiffness, fluid resistivity and the stochastic Brownian force, respectively. It is assumed that both particle and trap reside at the origin of the coordinate system at t = 0 (*i.e.* $w(0) = X(0) = 0$). The Fourier transform of eqn (2) is

$$0 = -\left(2\pi i\omega\hat{R}(\omega) + \kappa\right)\hat{w}(\omega) - 2\pi i\omega\hat{R}(\omega)\hat{X}(\omega) + \hat{F}_B(\omega) \quad (3)$$

Applying the formalism of Mason and Weitz, the fluid's resistance is related to its complex viscosity $\hat{\eta}(\omega)$ and particle radius (a) by the generalized Stokes equation, $\hat{R}(\omega) = 6\pi a\hat{\eta}(\omega)$.[8]

Multiplying eqn (3) by the complex conjugate of trap position yields

$$0 = \left(1 + \frac{\xi}{2\pi i\omega\tilde{\eta}}\right)\hat{C}_{wx}(\omega) + \hat{S}_{xx}(\omega) \quad (4)$$

ξ denotes the characteristic optical stress, $\frac{\kappa}{6\pi a}$. The cross-power spectral density $\hat{C}_{wx}$, and power spectral density $\hat{S}_{xx}$, are the frequency-space representations of the cross- and auto-correlation functions, $\langle \hat{w}\hat{X}^* \rangle$ and $\langle \hat{X}\hat{X}^* \rangle$, respectively (brackets denote time-averaged quantities). The thermal force term is nullified because it is uncorrelated with trap position. The ratio $-\hat{C}_{wx}/\hat{S}_{xx}$ defines the fluid's response function, $\hat{H}(\omega)$. Substituting into 4 and rearranging gives a straightforward expression for the fluid's complex modulus ($\hat{G}(\omega) = 2\pi i\omega\hat{\eta}$).

$$\hat{G}(\omega) = \frac{\xi\hat{H}(\omega)}{1 - \hat{H}(\omega)} \quad (5)$$

The FM input scans the band $[\omega_c \pm \omega_\Delta]$ in an analog manner. However, the signal's power is stored at discrete frequencies, spaced by ω_m, which have a one-to-one mapping onto the output for linear time-invariant systems. Filtering is required to sift out the activated spectrum. This can be done, for example, by thresholding the power spectral density of the drive signal, as shown in Fig. 3, or applying simple peak finding algorithms. Since the input signal has a known Fourier decomposition with coefficients given by a series of first-order Bessel functions, more sophisticated filtering procedures are feasible. However, simple filtering procedures are sufficient for the scope of this work.

FMMR and other active techniques are effectively limited at high frequencies by the compliance of the optical trap. Probe displacement and trap position converge as the forcing frequency is increased. The disparity between these quantities ultimately falls below the resolution of the detector for $\omega \gg \omega_k$, where the trap corner frequency $\omega_k = 2\xi\pi\hat{\eta}(0)$, prohibiting measurement of viscoelasticity. In light of this limitation, all maximum frequency of all FM inputs was limited to ~3 kHz, despite the fact that the Nyquist frequency was 20 kHz in all measurements.

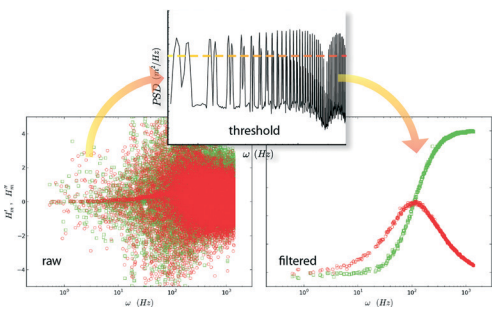

Fig. 3 Filtering procedure for FMMR measurements. The power spectrum (middle) from the trap's positional signal is thresholded to to filter the raw response function.

Results & discussion

Newtonian fluids

Newtonian fluids exhibit a purely dissipative stress response due to the properties of constant viscosity and zero elasticity. Under these conditions, resistivity is equivalent to the Stokes' drag coefficient, $R = 6\pi\eta a$. The response function for a Newtonian fluid is

$$\hat{H}(\omega) = \frac{\omega^2 + i\omega\omega_k}{\omega_k^2 + \omega^2} \quad (6)$$

Measurements in water were performed with $\omega_m = 0.7$ Hz, $\mathcal{M} = 2142.1$ and $\mathcal{C} = 2142.9$. The trap corner frequency, extracted from the calibration, was 110 Hz. The complex response function ($\hat{H} = H' + iH''$) obtained *via* FMMR is in excellent agreement with eqn (6) (Fig. 4).

The complex modulus obtained for water is shown in the inset of Fig. 4. The imaginary component, G'', scales as ~ω, consistent with a Newtonian fluid. Similar to the 'wideband microrheology' method devised by Preece *et al.*,[21] systematic and experimental noise sources give rise to elastic artifacts in Newtonian fluids. Drift and laser laser pointing instability can compromise the FMMR measurement at low frequency ($\lesssim$10 Hz), where probe displacement is small. The positive G' values clustered around 120 Hz arise due to AC electronic noise in the AOD power supply. Viscous drag increases with the speed at which the trap is rastered, causing the displacement amplitude registered by the detector to approach that of the drive signal. The disparity between the input and output amplitudes ultimately falls below the detector's resolution, limiting measurement accuracy at high frequency ($\omega \gg \omega_k$).

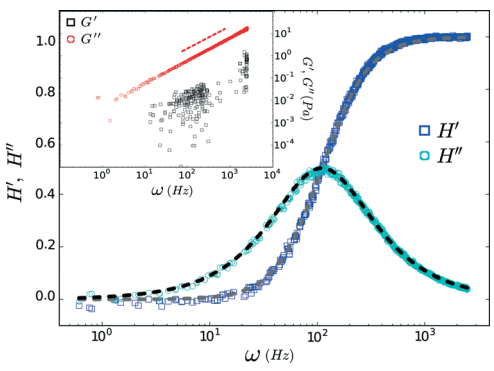

Fig. 4 Response function measured in water. Dashed lines denote H' (gray) and H'' (black) from eqn (6) plotted with a corner frequency of 110 Hz. The inset shows the corresponding complex modulus and the dashed line represents the expected scaling for the loss modulus.

Dividing the loss modulus by $2\pi i\omega$ yields a constant viscosity (Fig. 5) of $\eta = 1.00 \pm 0.09$ mPa s (mean ± standard deviation). These results are in excellent agreement with the known value (0.97 mPa s) for water at $T = 22$ °C, demonstrating the accuracy and efficacy of FMMR.

Viscoelastic materials

FMMR measurements in aqueous PEO (200 kDa) were performed with a polymer weight fraction of 5% w/w, an order-of-magnitude beyond the concentration threshold for viscoelastic behavior.

The viscoelastic behavior of the polymer solution conforms to the single-mode Maxwell model (Fig. 6).[26,32] The viscous modulus dominates below 500 Hz and displays an asymptotic scaling $\sim\omega$, while the storage modulus roughly scales as $\sim\omega^2$ for frequencies in the range of 10–100 Hz.

The minimum shear modulus that can be determined from oscillatory measurements is constrained by the probe's thermal energy, k_BT, and s, the spatial resolution of the QPD (ESI†).

$$\hat{G}^* \approx \frac{1}{2(A-s)^2}\left(3\pi\xi s^2 + \frac{k_BT}{a}\right) \quad (7)$$

The parameter settings for experiments in PEO were $\xi = 0.57$ Pa, $A = 0.25$ μm and $s \approx 10$ nm, leading to $G^* \approx 0.04$ Pa. G' falls outside of the effective measurement range below ~5 Hz. G', is also particularly impacted by the systematic noise sources noted earlier, due to the fluid's weakly elastic nature. In spite of these complications, the data in Fig. 6 is consistent with previous results published by Dasgupta *et al.*[26]

The instrument limitations described above, can potentially be circumvented by exploiting FMMR's capability to conduct high-resolution, wide-band scans. The Kramers–Kronig relation can be invoked to indirectly obtain G' by integrating G''.[8,27]

The applicability of FMMR to advanced, functional materials is demonstrated by measurements performed on recombinant type-III human collagen.[28] The biopolymer is engineered with specific sites for intermolecular bonding through either direct coupling between macromolecules or bridging with a cross-linking reagent. This design enables the material's rheology to be optimized for various applications in tissue engineering and drug-delivery, using levers such as site density, ionic strength, pH and cross-linker valency and rigidity.[29]

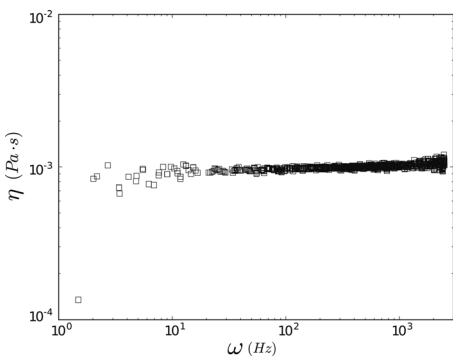

Fig. 5 Water viscosity measured by FMMR.

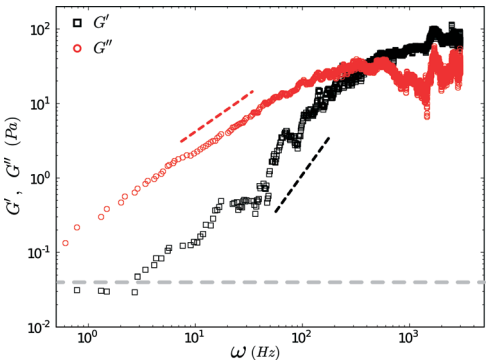

Fig. 6 Complex modulus of 5% w/w aqueous 200 kDa PEO measured using $\omega_m = 0.7$ Hz, $\mathcal{C} = 2142.9$ and $\mathcal{M} = 2142.1$. Data have been smoothed by applying a moving average. The black and red dashed lines indicate expected asymptotic frequency scalings for storage ($\sim\omega^2$) and loss ($\sim\omega$) moduli in an ideal Maxwell fluid, respectively. The grey line shows the lower limit for the modulus measurement.

The rheology of a 1.2 mg ml^{-1} recombinant collagen solution was measured 42.5 and 45 hours after the addition of a multi-valent cross-linker using FMMR (Fig. 7). The biopolymer solution becomes increasingly viscoelastic over time, as indicated by the vertical shift in the shear modulus. Both storage and loss components exhibit fractional power-law growth with respect to frequency, consistent with theoretical descriptions of entangled polymer networks. Such scaling behavior in collagen gels and other biopolymer systems has been reported previously,[13,27,30,31] and results obtained by FMMR are consistent with recently reported bulk rheology.[29]

The FMMR results are validated by data obtained during trap calibration. The SIR technique doubles as a non-oscillatory form of microrheometry.[21,24] The shear modulus

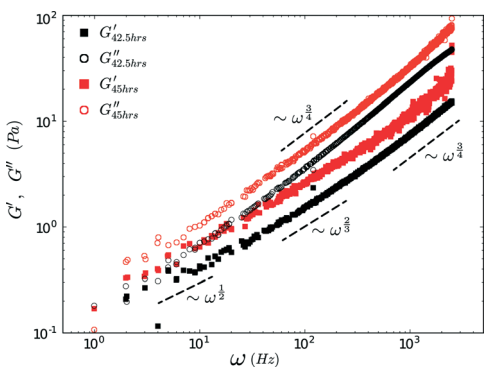

Fig. 7 Complex modulus of recombinant collagen (1.2 mg ml^{-1}) in 5 mM HEPES buffer (pH 5) measured by FMMR at 42.5 and 45 hours after addition of a 4-arm cross-linker (0.2 mM). FMMR was performed with $\omega_m = 1$ Hz $\mathcal{C} = 1250$ and $\mathcal{M} = 1249$.

extracted from the probe's step-response overlaps with oscillatory measurements of the biopolymer's rheology (ESI†).

Frequency modulation *versus* frequency sweep

Measurement dynamics for the FM and FS schemes were evaluated through simulations in a Maxwell fluid, with complex viscosity[32]

$$\hat{\eta}(\omega) = \eta_\infty + \frac{K_\infty \tau_M}{1 - 2\pi i \omega \tau_M} \tag{8}$$

The material has a constant elastic modulus K_∞, and background solvent viscosity η_∞. The Maxwell time, τ_M, dictates the time-scale for viscous reentrance. All simulation runs were performed using $K_\infty = 100^{-2}$ Pa, $\eta_\infty = 10^{-2}$ Pa s, $\tau_m = 10^{-3}$ s and $\xi = 0.53$ Pa ($\kappa = 10^{-5}$ N m^{-1}). The system's response function was derived by converting $\hat{\eta}$ to $\hat{G}$ and substituting into eqn (5). Brownian probe fluctuations were emulated by adding Gaussian noise to the output of each run. Fig. 8 illustrates how a simulated FM measurement converges over time.

Transient behavior in FMMR and sweep measurements were examined using the Allan variance of probe position.[33] Originally developed to evaluate the stability of clocks and oscillators,[34] this analysis can be used to optimize measurements subject to stochastic and systematic noise.[35] Allan variance is defined as the average-square differential between the means of sequential subsets in a time-series.

$$\sigma^2(\tau) = \frac{1}{2}\left\langle \left(\bar{w}_{i+1} - \bar{w}_i\right)^2 \right\rangle \tag{9}$$

The number of data points, n, used to evaluate each local mean $\bar{w}_i$, determines the corresponding measurement lag-time, $\tau = \frac{n}{f_s}$ (f_s is the measurement sampling frequency). The brackets $\langle\cdot\rangle$ in eqn (9) denote an arithmetic average. The Allan deviation ($\sigma(\tau)$) provides a measure of the statistical uncertainty in particle position, which directly dictates the accuracy of the rheological parameters discerned by microrheology. Because τ represents a block averaging time, the corresponding absolute time is a multiple of τ.

The probe's Brownian motion defines a lower bound for uncertainty in particle position ($\sigma_L(\tau) \sim \tau^{-\frac{1}{2}}$). Oscillating the particle generates periodic perturbations from this thermal limit (Fig. 9), the amplitude ($\Delta\sigma = \sigma - \sigma_L$) of which decays as $\sim \frac{1}{\omega\tau}$.[33] The total time required for a piecewise sweep is simply the sum of all individual measurement periods.

$$t_{fs}^* \propto \frac{1}{\omega_c}\left(1 + 2\sum_{n=1}^{\mathcal{M}} \frac{1}{1 - \left(\frac{n}{\mathcal{C}}\right)^2}\right) \tag{10}$$

Similar settling behavior is observed with FMMR under all parameter settings (Fig. 9), for $\tau \gtrsim \frac{1}{\omega_m(\mathcal{C} - \mathcal{M})}$. Thus, t^* for FMMR measurements is inversely proportional to the lowest active frequency (Fig. 10).

$$t_{fm}^* \propto \frac{1}{\omega_m(\mathcal{C} - \mathcal{M})} \tag{11}$$

The ratio between t_{fs}^* and t_{fm}^* defines a relative efficiency metric, Γ

$$\Gamma \sim \left(1 - \frac{\mathcal{M}}{\mathcal{C}}\right)\left(1 + 2\sum_{n=1}^{\mathcal{M}} \frac{1}{1 - \left(\frac{n}{\mathcal{C}}\right)^2}\right) \tag{12}$$

The summation $\sum \frac{1}{1-\left(\frac{n}{\mathcal{C}}\right)^2} \approx \mathcal{M}$ when $\mathcal{M}/\mathcal{C}$ is small, leading to $\Gamma \approx 1 + \frac{\mathcal{M}}{\mathcal{C}}\left(2(\mathcal{C} - \mathcal{M}) - 1\right)$, which, as expected, reaches unity as $\mathcal{M}/\mathcal{C} \rightarrow 0$. Fig. 11 shows Γ is non-monotonic but greater

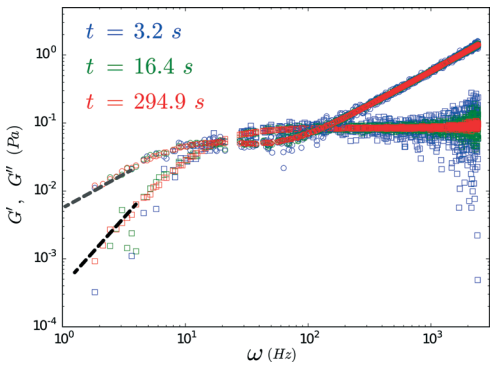

Fig. 8 Complex modulus components G' (squares) and G'' (circles) obtained at various time points from FMMR measurements simulated in a Maxwell fluid. The FM parameters for the run were $\mathcal{M}$ = 1225, $\mathcal{C}$ = 1273 and ω_m =1.1 Hz. The black (~ω^2) and gray (~ω) lines indicate the asymptotic power-law behavior expected for the storage and loss moduli respectively.

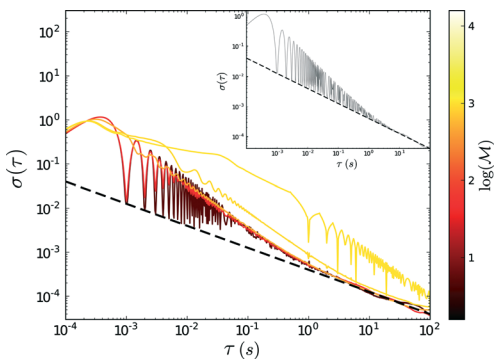

Fig. 9 Allan deviation tabulated from simulated FMMR measurements. The plotted data were obtained with ω_m = 1 Hz and $\mathcal{C}$ = 1000. The inset shows the allan deviation results for $\mathcal{M}$ = 0 (single-mode case). Dashed lines represent the thermal limit (~$\tau^{1/2}$).

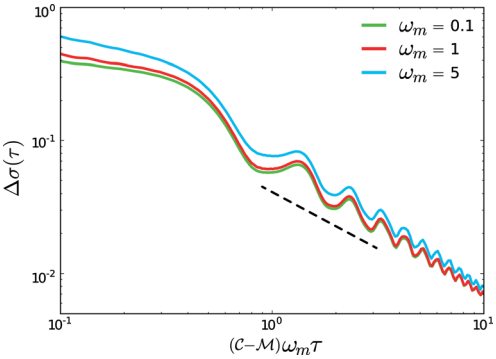

Fig. 10 Allan deviation, with thermal limit subtracted, from FMMR measurements with $\mathcal{C} = 10^3$ and $\mathcal{M} = 900$. The modulation frequency and frequency bounds were varied in each run. The dashed line corresponds to a power-law decay of −1.

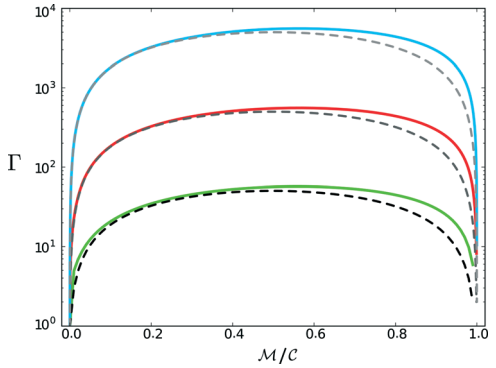

Fig. 11 Convergence time ratio between analogous frequency sweep and frequency modulation measurements. Solid lines denote numerically tabulated results from eqn (12) with $\mathcal{C} = 10^2$ (green), 10^3 (red), and 10^4 (blue). Dashed lines show the analytical result when the summation is approximated as $\mathcal{M}$.

than unity for $\mathcal{M}/\mathcal{C} \in (0, 1)$. The relative disparity in measurement speed can span several orders in magnitude, increasing with both resolution and bandwidth. Thus, FMMR is a more efficient approach to active microrheology.

Conclusions

FMMR parallelizes numerous single-mode measurements enabling rheological characterization over several frequency decades in a single pass. The technique operates with increased speed relative to the standard, linear sweep approach without compromising accuracy. FMMR provides tunable resolution and bandwidth, and is likely amenable to non-linear measurement because the active drive frequencies are known *a priori*.

The rapidity and versatility of FMMR not only expands the applicable scope of active microrheology, but has notable industrial implications as well. The technique is simple to implement and can serve as the functional kernel for advanced microrheology instrumentation capable of highly automated operations and live display of a material's complex modulus. FMMR is particularly suited for materials that are difficult or costly to produce, and must be characterized over a broad parameter space. Emulating the μ^2 rheology technique devised by Schultz and Furst,[2] an FMMR-capable optical tweezer could be coupled with droplet microfluidics to create a system for high-throuput screening of biopharmaceutical, biomaterial and nanomaterial formulations.[36] There is tremendous value inherent in such technology, since optimizing multi-variate formulations prior to scale-up can expedite commercialization, streamline manufacturing and curtail unanticipated cost overruns. Frequency modulation may have a number of non-rheological applications as well. AC and pulsed electric or magnetic fields instigate a variety of organizational and kinematic phenomena within colloidal dispersions, depending on particle size, shape and chemistry.[37–39] The strength and frequency of the applied field govern the equilibrium microstructure and kinetic stability of non-equilibrium phases by regulating the intricate balance between thermodynamic interactions and particle mobility. FM may offer a tractable mechanism of control over self-assembly, transport and separation processes by providing a means of precisely sculpting a colloidal system's energy landscape.[40] Encoding organization through a prescribed modulator signal is particularly intriguing,as it would facilitate scalable manufacturing of micro- and nano-structured materials with tailored physical, mechanical and thermal transport properties.

Acknowledgements

We thank Dr. S.-W. Wang and R. Que for providing recombinant collagen and acknowledge International Fragrances and Flavors for financial support of this project.

References

1 T. M. Squires and T. G. Mason, *Annu. Rev. Fluid Mech.*, 2010, **42**, 413.
2 K. M. Schultz and E. M. Furst, *Lab Chip*, 2011, **11**, 3802.
3 T. Savin and P. S. Doyle, *Soft Matter*, 2007, **3**, 1194.
4 W. A. Petka, J. L. Harden, K. P. McGrath and D. Wirtz, *Science*, 1998, **281**, 389.
5 W. Mulyasasmita, J. S. Lee and S. C. Heilshorn, *Biomacromolecules*, 2011, **12**, 3406.
6 N. Yamaguchi, L. Zhang, B. S. Chae, C. S. Palla, E. M. Furst and K. L. Kiick, *J. Am. Chem. Soc.*, 2007, **129**, 3040.
7 C. Yan and D. J. Pochan, *Chem. Soc. Rev.*, 2010, **39**, 3528.
8 T. G. Mason and D. A. Weitz, *Phys. Rev. Lett.*, 1995, **74**, 1250.
9 M. Tassieri, R. M. L. Evans, R. L. Warren, N. J. Bailey and J. M. Cooper, *New J. Phys.*, 2012, **14**, 115032.
10 M. T. Valentine and H. D. Ou-Yang, *J. Phys.: Condens. Matter*, 1996, **8**, 9477–9482.
11 D. Velegol and F. Lanni, *Biophys. J.*, 2001, **81**, 1786–1792.
12 E. M. Furst, *Curr. Opin. Colloid Interface Sci.*, 2005, **1**, 79.
13 T. A. Waigh, *Rep. Prog. Phys.*, 2004, **68**, 685.

14 M. Tassieri, T. A. Waigh, J. Trinick, A. Aggeli and R. M. L. Evans, *J. Rheol.*, 2010, **54**, 117.
15 A. Yao, M. Tassieri, M. Padgett and J. Copper, *Lab Chip*, 2009, **9**, 2568.
16 L. G. Wilson and W. C. K. Poon, *Phys. Chem. Chem. Phys.*, 2011, **13**, 10617.
17 I. Sriram, R. DePuit, T. M. Squires and E. M. Furst, *J. Rheol.*, 2009, **53**, 357.
18 F. Ziemann, J. Rädler and E. Sackmann, *Biophys. J.*, 1994, **66**, 2210.
19 L. A. Hough and H. D. Ou-Yang, *Phys. Rev. E: Stat., Nonlinear, Soft Matter Phys.*, 2006, **73**, 031802.
20 H. Lee, Y. Shin, S. T. Kim, E. L. Reinherz and M. J. Lang, *Appl. Phys. Lett.*, 2012, **101**, 031902.
21 D. Preece, R. Warren, R. M. L. Evans, G. M. Gibson, M. J. Padgett, J. M. Cooper and M. Tassieri, *J. Mod. Opt.*, 2011, **13**, 044022.
22 E. E. Holly, S. K. Venkataraman, F. Chambon and H. H. Winter, *J. Non–Newtonian Fluid Mech.*, 1988, **27**, 17–26.
23 M. In and R. K. Prud'homme, *Rheologica Acta.*, 1993, **32**, 556–565.
24 M. M. Shindel, J. W. Swan and E. M. Furst, *Rheol. Acta*, 2013, **52**, 455.
25 F. Gittes and C. Schmidt, *Opt. Lett.*, 1998, **23**, 7.
26 B. R. Dasgupta, S. Y. Tee, J. C. Crocker, B. J. Frisken and D. A. Weitz, *Phys. Rev. E: Stat., Nonlinear, Soft Matter Phys.*, 2002, **5**, 051505.
27 D. Mizuno, D. A. Head, F. C. MacKintosh and C. F. Schmidt, *Macromolecules*, 2008, **41**, 7194.
28 S. W. P. Chan, S.-P. Hung, S. Raman, G. W. Hatfield, R. Lathrop, N. A. Da Silva and S.-W. Wang, *Biomacromolecules*, 2010, **11**, 1460.
29 R. Que, A. Mohraz, N. A. Da Silva and S.-W. Wang, *Biomacromolecules*, 2014, **15**, 35403549.
30 M. Shayegan and N. R. Forde, *PLoS One*, 2013, **8**, e70590.
31 B. Schnurr, F. Gittes, F. C. MacKintosh and C. F. Schmidt, *Macromolecules*, 1997, **30**, 7781.
32 M. Grimm, S. Jeney and T. Franosch, *Soft Matter*, 2011, **7**, 2076.
33 M. Andersson, F. Czerwinski and L. B. Oddershede, *J. Opt.*, 2011, **13**, 044020.
34 D. W. Allan, *Proc. IEEE*, 1966, **54**, 221.
35 F. Czerwinski, A. C. Richardson and L. B. Oddershede, *Opt. Express*, 2009, **17**, 13255.
36 K. M. Schultz, A. V. Bayles, A. D. Baldwin, K. L. Kiick and E. M. Furst, *Biomacromolecules*, 2011, **12**, 4178.
37 J. M. McMullan and N. J. Wagner, *Soft Matter*, 2010, **6**, 5443.
38 M. Grzelczak, J. Vermant, E. M. Furst and L. M. Liz-Marzán, *ACS Nano*, 2010, **4**, 3591.
39 J. W. Swan, P. A. Vasquez, P. A. Whitson, E. M. Fincke, K. Wakata, S. H. Magnus, F. De Winne, M. R. Barratt, J. H. Agui, R. D. Green, N. R. Hall, D. Y. Bohman, C. T. Bunnell, A. P. Gast and E. M. Furst, *Proc. Natl. Acad. Sci. U. S. A.*, 2012, **109**, 16023.
40 S. Torquato, *Soft Matter*, 2009, **5**, 1157.

